HHS Public Access

Author manuscript

Tissue Eng. Author manuscript; available in PMC 2016 April 04.

Published in final edited form as:

Tissue Eng. 2006 February ; 12(2): 413–421. doi:10.1089/ten.2006.12.413.

Characterizing Nanoscale Topography of the Aortic Heart Valve Basement Membrane for Tissue Engineering Heart Valve Scaffold Design

SARAH BRODY, B.E.[1,2], **THAPASIMUTHU ANILKUMAR, M.V.Sc., Ph.D.**[1], **SARA LILIENSIEK, Ph.D.**[3], **JULIE A. LAST, Ph.D.**[4], **CHRISTOPHER J. MURPHY, D.V.M., Ph.D.**[3], and **ABHAY PANDIT, B.E., M.S., M.P.H., Ph.D.**[1,2]

[1]National Centre for Biomedical Engineering Science, National University of Ireland, Galway, Ireland. [2]Department of Mechanical and Biomedical Engineering, National University of Ireland, Galway, Ireland. [3]Department of Surgical Sciences, School of Veterinary Medicine, University of Wisconsin-Madison, Madison, Wisconsin. [4]Engineering Physics Department, University of Wisconsin-Madison, Madison, Wisconsin.

Abstract

A fully effective prosthetic heart valve has not yet been developed. A successful tissue-engineered valve prosthetic must contain a scaffold that fully supports valve endothelial cell function. Recently, topographic features of scaffolds have been shown to influence the behavior of a variety of cell types and should be considered in rational scaffold design and fabrication. The basement membrane of the aortic valve endothelium provides important parameters for tissue engineering scaffold design. This study presents a quantitative characterization of the topographic features of the native aortic valve endothelial basement membrane; topographical features were measured, and quantitative data were generated using scanning electron microscopy (SEM), atomic force microscopy (AFM), transmission electron microscopy (TEM), and light microscopy. Optimal conditions for basement membrane isolation were established. Histological, immunohistochemical, and TEM analyses following decellularization confirmed basement membrane integrity. SEM and AFM photomicrographs of isolated basement membrane were captured and quantitatively analyzed. The basement membrane of the aortic valve has a rich, felt-like, 3-D nanoscale topography, consisting of pores, fibers, and elevations. All features measured were in the sub-100 nm range. No statistical difference was found between the fibrosal and ventricular surfaces of the cusp. These data provide a rational starting point for the design of

Address reprint requests to: Prof. Abhay Pandit, Department of Mechanical and Biomedical Engineering, National University of Ireland, Galway, Ireland abhay.pandit@nuigalway.ie.

This work was performed at the University of Wisconsin-Madison and at the National University of Ireland, Galway, Ireland.

Abstracts of this study have appeared in the following: Identification of nanotopography for aortic valve scaffold design. Proceedings of Joint Meeting of Tissue Engineering Society International and the European Tissue Engineering Society. Lausanne, Switzerland, October 2004; Nanoscale topography of aortic valve basement membrane. A novel approach to tissue engineering scaffold design. Proceedings of The 28th Annual Microscopy Society of Ireland Meeting. Dublin, Ireland, September 2004; Nanotopography of the aortic valve basement membrane with a view to tissue engineering scaffold design. Proceedings of Advances in Tissue Engineering and Biology of Heart Valves. Florence, Italy, September 2004; Identification of nanoscale topography for aortic valve scaffold design. Proceedings of 7th World Biomaterials Congress. Sydney, Australia, May 2004.

extracellular scaffolds with nanoscale topographic features that mimic those found in the native aortic heart valve basement membrane.

INTRODUCTION

Aortic valve disease, which can lead to heart failure, constitutes a high percentage of cardiovascularrelated deaths. Every year approximately 60,000 mechanical and bioprosthetic aortic heart valve replacements are implanted in the United States and 170,000 worldwide.[1] Implantation of mechanical and bioprosthetic valves is the most commonly utilized method for the treatment of heart valve disease. Although mechanical heart valves perform well, long-term they are associated with thrombogenic responses, necessitating life-long anticoagulation therapy for recipients.[2] Bio-prosthetic heart valves have superior hemodynamic characteristics but are limited by their short lifespan and tendency to calcify.[2] Neither current therapy for heart valve replacement addresses the need for growth potential in patients, specifically in pediatric aortic heart valve replacements. Therefore, current research trends are focusing on the development of tissue-engineered heart valves (TEHV). This study seeks to optimize parameters for the scaffold design aspect of TEHV, and, in particular, the characterization of design parameters that will optimize endothelial cell growth on the scaffold surface. Topography of the aortic heart valve basement membrane is an essential scaffold design parameter that has not yet been addressed.

The basement membrane, located on the ventricular and fibrosal sides of the heart valve, is a thin (20–100 nm), self-assembled, sheet-like structure through which the endothelial cells associate with the underlying stromal elements. The basement membrane provides structural support, divides tissues into various compartments, and regulates cell behavior.[3,4] Previous research has established that basement membranes are comprised mainly of extracellular matrix proteins, proteoglycans, and glycoproteins, such as collagen (type IV) and laminin.[3,5] The basement membrane also serves as a reservoir for soluble trophic factors. Detailed analysis of corneal and bladder basement membranes documented a rich three-dimensional (3-D) architecture consisting of a meshwork of pores, fibers and elevations.[6–9] In addition to its structural role, the basement membrane influences cellular behavior by providing a suitable topography for cellular attachment.

The study of cellular response to micro-topography has been substantial[10–15]; however, recent work has demonstrated that the basement membrane is composed of nanoscale features and that the major impact of topographic cueing occurs with these nanoscale features.[16,17] Previous studies have shown that contact with nanoscale features increases both cell density[18] and cell spreading during the initial cell culture stages. This creates a more biomimetic confluent layer of endothelial cells than that observed on smooth surfaces.[19] Nanoscale topographic features have recently been shown to modulate cell adhesion, spreading, focal adhesion formation, orientation, proliferation, differentiation, and migration in other cell lines.[16,17,20] Surface elevations ranging between 13 and 95 nm have been shown to increase endothelial spreading, with the largest cellular response seen on the smallest 13 nm feature sizes.[21] Nanoscale roughness also enhances adhesion and growth of endothelial cells.[22] Identification of the nanoscale basement membrane surface topography,

upon which the endothelial cells of the aortic heart valve grow, provides a rational basis for TEHV scaffold design.

This paper reports on a technique for de-endothelialization of the aortic heart valve that preserves the integrity of the basement membrane. The process by which two independent but complementary imaging techniques, scanning electron microscopy (SEM) and atomic force microscopy (AFM), were used to investigate features of the basement membrane, such as pore depth, pore diameter, fiber diameter, and elevation height, is also reported. The ventricular and fibrosal surfaces of the valve are exposed to differing forces as the valve opens and blood leaves the heart; therefore, the study also investigated whether these differing conditions are reflected in the size or type of topographical features of the basement membrane.

MATERIALS AND METHODS

Aortic heart valves were harvested from 12- to 18-month-old market-weight pigs and dissected within 90 min of slaughter. All cusps were washed in Sorenson's buffer prior to removal of the endothelium. All reagents, unless otherwise stated, were purchased from Sigma-Aldrich (Dublin, Ireland). A schematic detailing the experimental procedure is provided in Figure 1. Preliminary studies on the removal of endothelial cells from the valve cusp, adapted from Abrams *et al.,*[6–9,23] involved varying combinations of ethylenediaminetetraacetic acid (EDTA) concentrations (1.5–7.5 mM) and incubation times in EDTA (5–180 min). The effects of sonicating (Brandson 3150, Branson Ultrasonics BV, Eemnes, The Netherlands) at a current of 2 A during the cellular removal process was also investigated. Following de-endothelialization all cusps were fixed for 2 h in either 2% glutaraldehyde/Sorenson's for SEM, AFM, and TEM analysis or 4% paraformaldehyde/phosphate-buffered saline (PBS) for light microscopy. Control cusps (not exposed to EDTA or sonication) were fixed identically immediately following dissection.

Verification of basement membrane integrity

Histological examination was carried out on both de-endothelialized ($n = 2$) and control samples ($n = 2$) in order to confirm the effectiveness of the cellular removal technique. Tissues were fixed and processed using standard techniques,[7] embedded in paraffin, sectioned at 6 μm, and stained with hematoxylin and eosin (H&E), Verhoeff's elastic, Masson's trichrome, and Alcian blue with periodic acid Schiff (PAS). The H&E stained sections were used to evaluate the efficiency of the endothelial cell removal technique while the other stains allowed investigation of the integrity of the remainder of the cusp tissue following the de-endothelialization process.

Immunolabeling for laminin, a basement membrane component, was also carried out on frozen sections of both de-endothelialized ($n = 2$) and control ($n = 2$) cusps to evaluate the integrity of the basement membrane following EDTA treatment. Cusps were cryopreserved in 20% sucrose/PBS for 12 h at 4°C following paraformaldehyde fixation. Tissues were embedded in Tissue Freezing Medium (Triangle Biomedical Sciences, Durham, NC) and sectioned at 6 μm. For immunhistochemical staining, sections were blocked with 3% normal goat serum (NGS)/PBS and incubated for 30 min. Sections were labeled with 50 μL of 1:40

dilution of rabbit anti-laminin (Sigma-Aldrich, St. Louis, MO) for 1 h followed by 30 min of incubation in goat anti-rabbit (IgG) secondary antibody (Alexa Fluor 594, Molecular Probes, Eugene, OR) at a concentration of 1:1000. Sections were counterstained with a nuclear dye, 4′-6-diamidino-2-phenylindole (DAPI), for 30 min. All incubations were carried out at room temperature in a moisture chamber. Frozen sections of human cornea were used as a positive control for laminin staining, and sections stained with secondary antibody alone were used as a negative control. Slides were viewed using rhodamine and DAPI filters on a fluorescence microscope (Axiovert 200M, Zeiss, Thornwood, NY).

Glutaraldehyde-fixed de-endothelialized ($n = 3$) and control cusps ($n = 1$) were examined by transmission electron microscopy. Asymmetrical samples (~2mm*3mm), cut from the central region of the cusps, allowed the fibrosal and ventricular surfaces of the cusp to be distinguished following processing. Samples were rinsed in Sorenson's buffer following initial glutaraldehyde fixation. Prior to resin infiltration, samples were post-fixed in 2% osmium tetroxide/Sorenson's for 1 h, dehydrated through several exchanges in graded alcohol (30-100%), rinsed in propylene oxide, and infiltrated in a 1:1 mixture of propylene oxide and resin overnight. The resin used was an approximate 1:1 mixture of Epon and Spurr (Polysciences, Warrington, PA), and samples were infiltrated in 100% resin following three to four 45 min washes. The samples were then embedded in resin-filled molds and allowed to harden overnight. Sections of 70–80 nm were cut using an ultramicrotome. To enhance the contrast of the TEM images, sections were stained with uranyl acetate for 10 min and then with lead citrate for an additional 10 min. Photomicrographs at various magnifications were taken (Philips CM120 TEM, Eindhoven, The Netherlands). Five photomicrographs from the fibrosal and ventricular sides of each sample were taken at a magnification of 30,000×. Photomicrographs of control and de-endothelialized samples were compared.

Scanning electron microscopy

Asymmetrical sections of de-endothelialized ($n = 3$) and control cusps ($n = 1$), as described for TEM analysis, were also used for SEM analysis. Two samples from the central region of each cusp were dehydrated in graded alcohols (30–100%) followed by several 15 min exchanges in absolute alcohol and critical point dried in CO_2. Samples were mounted on carbon stubs, and a 4 nm coating of gold was then applied using the ion-beam sputter coater (VCR Group, San Francisco, CA). A low-voltage, high-resolution SEM (S-4700 Hitachi Scientific Instruments, Berkshire, England) was used at 15 kV to capture images at various magnifications ranging from 300 to 30,000 ×. Stereo pairs at ±5° and at a magnification of 30,000× were also taken from the de-endothelialized samples. Three-dimensional measurements of the basement membrane, such as elevation heights and pore depths, were quantified using the formula:

$$\mathrm{Z} \quad 5 \quad \mathrm{P}/2Sin\,(\mathrm{a}/2)$$

where Z is the feature height, P is the parallax, and α is half of the angle of the stereo pair. Three random areas on both sides of each de-endothelialised sample were examined, resulting in 18 sets of stereo pairs. From each of the 18 stereo pairs, 10 pore depth and 10

elevation height measurements were calculated, and from the 0° image of each stereo pair 10 fiber diameter and 10 pore diameter measurements were taken using image analysis software (Image Pro, Media Cybernetics, Berkshire, England). All measurements were taken from random locations on the images, and statistical tables were used to choose the random location.

SEM photomicrographs taken at a magnification of 2,000 × were also used to quantify the effects of the de-endothelialization treatment in terms of percentage decrease in the number of cells on the valve surface. Both sides of control ($n = 1$) and de-endothelialized ($n = 3$) samples were examined, and three photomicrographs were captured per side. Cells in each photomicrograph were then counted and the number of cells present on de-endothelialized samples was compared to those of control samples.

Atomic force microscopy

Atomic force microscopy (AFM) images of the fibrosal and ventricular surfaces of 2% glutaraldehyde fixed de-endothelialized and control cusps were captured ($n = 3$) (NanoScope IIIa Multimode, Digital Instruments, Santa Barbara, CA). Images were acquired in tapping mode in solution using a commercially available liquid cell (Digital Instruments) with 120 μm oxide sharpened silicon nitride V-shaped cantilevers. The nominal spring constant of the cantilever was 0.35 N/m. Tissue samples were attached to the puck using a small drop of adhesive (Loctite, Super BonderR 495 Instant Adhesive, Rocky Hill, CT), which was allowed to dry for several minutes. A small drop of buffer PBS placed on the top surface of the tissue prior to assembling the liquid cell prevented tissue dehydration. Images for each sample were obtained on the basement membrane surface, one image of the fibrosal side and one image of the ventricular side, and were collected with the J scanner, which has a maximum range of 125 μm by 125 μm, operating at a scan rate of 2 Hz. The images were collected with 256 data points per line. All measurements were obtained in PBS, samples were taken from the central region of the cusp, and images were captured of random locations. Dimensional measurements such as pore depth, elevation height, fiber diameter, and pore diameter were taken using image analysis software (Image Pro).

RESULTS

Verification of basement membrane integrity

Varying conditions for effective de-endothelialization were assessed, and it was established that optimal conditions for endothelial cell removal on the porcine aortic valve cusps were 15 min in 2.5 mM EDTA followed by 1.5 min of sonication at 2 A in 2.5 mM EDTA. Both histological and immunohistochemical analyses verified that the basement membrane was not damaged as a result of the de-endothelialization process.

Sections of porcine aortic valve from control and EDTA treated tissues were stained with H&E to investigate the overall tissue integrity and presence or absence of endothelial cells. Our observations indicated that the monolayer of endothelial cells present on the control samples is predominantly removed post de-endothelialization (Fig. 2). Examination of sections stained with Masson's trichrome, Verhoeff's elastin, and Van Gieson stain verified

the preservation of normal cusp stromal anatomy following de-endothelialization. Alcian blue with PAS is a commonly used stain for the basement membrane. The periodic acid, a strong oxidizing agent, is thought to liberate aldehydes from polysaccharides, thereby allowing the Schiff reaction to stain the sites of liberation on the polysaccharides. It is believed that reticular fibers are the PAS-positive component of the basement membrane.[24] Examination of alcian blue with PAS-stained sections verified that the integrity of the basement membrane was preserved following de-endothelialization (Fig. 3).

An antibody to laminin, an established basement membrane component, was used to thoroughly characterize the presence of intact basement membrane. Frozen sections of both control and de-endothelialized sections stained with anti-laminin stained positive in both de-endothelialized and control cases, further confirming the presence of a continuous layer of basement membrane following EDTA treatment.

TEM photomicrographs taken at magnifications ranging from 1,000 to 30,000 × prior to and following basement membrane isolation provided further confirmation of the successful removal of the endothelial cell monolayer and preservation of the basement membrane layer.

Characterization of basement membrane topography

SEM photomicrographs provided high-magnification images of the rich nanoscale topography of the basement membrane surface on both sides of the aortic heart valve. Figure 4A highlights three layers of the heart valve: a monolayer of endothelial cells lying on the basement membrane and the underlying extracellular matrix. The basement membrane, as indicated by the square on Figure 4A, was examined at higher magnifications (Fig. 4B). The photomicrographs taken at 30,000 × were used in conjunction with image analysis software to quantify features such as pore diameter and fiber diameter on the surface. Pore diameters measured ranged from 7 to 98 nm, with an average of 32 ± 2 nm and 28 ± 4 nm on the ventricular and fibrosal sides, respectively. Fiber diameters ranging from 6 to 94 nm with averages of 28 ± 3nm and 30 ± 2 nm on the ventricular and fibrosal sides, respectively, were measured (Table 1). Pore depth and elevation height measurements were taken using the stereo pair images, which formed “virtual” 3-D images of the basement membrane topography. For each feature type analyzed, ten measurements were taken from each image, resulting in a total of 30 measurements from each side of each sample. Pore depths ranged from 4 to 89 nm, with an average of 22 ± 13 nm and 22 ± 14nm on the ventricular and fibrosal sides, respectively, and elevation heights ranged from 4 to 71 nm, with averages of 26 ± 13 nm and 22 ± 11 nm on the ventricular and fibrosal sides, respectively (Table 1). Student *t* tests verified that there is no statistical difference ($p < 0.05$) between feature sizes on the fibrosal and ventricular sides for any feature type analyzed. Additionally SEM images were used to quantify the percentage of cells removed through the cellular removal technique. It was found that 80% of the cells were removed from the surface of the cusp following de-endothelialization.

Atomic force microscopy was performed as a complimentary technique to increase the robustness of the quantitative data set. The use of both SEM and AFM decreases the potential for introduction of confounding variables associated with either method individually. For each feature type analyzed 10 measurements were taken from each image

(Fig. 5). Overall, mean pore diameter was 25.8 ± 3 nm with a range of 8 to 59 nm and mean fiber diameter was 32.4 ± 1 nm with a range of 24 to 51 nm. Overall, mean elevation height and pore depth measurements were 2.8 ± 0.04 nm and 5.7 ± 0.3 nm, respectively, and measurements for elevation height and pore depth ranged from 1 to 10 nm and 2 to 10 nm, respectively. No statistical difference ($p < 0.05$) was found between the two surfaces. Similar findings to those found with the SEM were found using AFM; all feature sizes were in the sub-100 nm range.

DISCUSSION

The removal of the endothelial layer of the porcine aortic valve without damage to the underlying basement membrane was critical to successfully characterizing the basement membrane topography. Various methods of removing cells from basement membranes have previously been investigated. Spurr and Gibson[23] carried out ultra-structural and immunohistochemical studies to compare the effects of dispase II and EDTA on the basement membrane zone of corneal epithelium. It was found that although dispase II, a bacterial neural protease, facilitates the removal of intact sheets of epithelium, EDTA cleanly separates the epithelial sheets from the basal laminae of the basement membrane. As an alternative method, Bjorling *et al.*[25] investigated the effectiveness of removing venous endothelium by the passage of a current of air over the cellular layer. It was reported that this is an efficient method of removing the endothelial cells since it did not affect the integrity of the underlying smooth muscle layer; however, the impact that this method has on the integrity of the basement membrane layer was not reported. De-endothelialization studies detailed in this paper were based on previous research by Abrams *et al.,*[6–9] where basement membrane isolation was successfully optimized for rhesus macaque bladder and for rhesus macaque, human, and canine cornea. The cellular layer lining these organs is similar to the delicate endothelial monolayer overlying the aortic valve basement membrane. The best conditions for de-endothelialization of the aortic valve cusp surface represented the optimum balance between cell removal and preservation of basement membrane integrity. Using optimized parameters, 80% of endothelial cells on the valve surface were removed.

Two distinctly different but complimentary imaging techniques, AFM and SEM, were used to quantitatively examine features in the basement membrane surface topography. These techniques each have their own specific advantages and were used in tandem to minimize the possible introduction of confounding variables associated with preparation techniques, such as fixation and dehydration. SEM lends itself to examining a large number of samples while AFM allows for basement membrane topographical analysis in the more physiologically relevant liquid state. Although glutaraldehyde was used to preserve samples for both techniques, previous studies in which an x-ray microscope was used to compare changes in morphology of various glutaraldehyde fixed and unfixed samples found that shrinkage due to glutaraldehyde fixation was below 15%.[26] A strong correlation was found between the two techniques for pore and fiber diameter measurements. SEM measurements for pore depth and elevation height were on average smaller than SEM measurements for pore and fiber diameters, a trend which, although more pronounced, is also reflected in the AFM results. Measurements, captured by both techniques, highlight the lack of uniformity

in basement membrane features and provide an accurate indication of the nanoscale environment in which endothelial cells on the heart valve surface grow *in vivo*.

The feature sizes of pore diameters, fiber diameters, and elevation heights reported for endothelial basement membranes from the human, macaque, and canine corneas, as well as the macaque bladder, were greater than those found for the aortic valve basement membrane. For the human and canine corneal endothelial basement membranes, reported mean feature sizes ranged from 31 (mean fiber diameter) to 192 nm (mean elevation height) and from 15 (mean fiber diameter) to 115 nm (mean elevation height), respectively.[6,9] Mean feature sizes on Matrigel (Collaborative Research, Bedford, MA), a commercially available basement membrane-like substrate, lay between 69 and 162 nm.[7] All aortic valve cusp basement membrane mean feature sizes were in the sub-100 nm range (Table 1). Mean fiber diameters measured in all studies were similar, which may be the result of the same fibrous basement membrane components, such as collagen or laminin, present in all basement membranes regardless of tissue or species.

Smaller pore diameters and elevation heights on the aortic valve basement membrane may be associated with differing environmental conditions and cell turnover rates. Differing, location-specific functions of endothelium may also play a role in the relationship between the endothelial cells and the basement membrane topography; in the cornea, endothelial cells and their underlying basement membrane (Descemet's membrane) are primarily responsible for pumping excess water from the cornea, while in the aortic heart valves, the endothelial cells and basement membrane primarily reduce thrombogenicity, thereby preventing coagulation of the blood.

As the aortic heart valve opens, the ventricular surface of the cusp is exposed to the full force of shear stress from systolic blood flow while the fibrosal surface is protected. It was therefore suspected that the basement membrane topography may reflect these differing *in vivo* conditions. However, no statistical difference was found between the two surfaces for any basement membrane feature analyzed. Our findings indicate that the difference in shear stress exerted on the two cusp surfaces, caused by the thrust of the blood out of the right ventricle during systole, does not influence basement membrane topography. These findings are supported by a study carried out on endothelial cell orientation on the aortic valve cusp.[27] Results of this study showed that endothelial cell orientation on the cusp, like basement membrane topography, is not a function of shear stress: cellular orientation on both the ventricular and fibrosal sides of the cusp is in the circumferential direction, and therefore, perpendicular to the direction of blood flow.

Vascular endothelial cells interface with a basement membrane characterized by complex nanoscale topography. Individual endothelial cells interact with thousands of individual topographic features. The fact that biologic length scale topographic features have been shown to strongly modulate a variety of fundamental cell behavior in diverse cell types[16,17,28] suggests that the incorporation of biologic length scale features should be considered in tissue engineering of scaffolds for use in development of valve equivalents. A study on epithelial cell response to a ridge and groove type substratum with pitches ranging from 400 to 4000 nm suggests that improved valve equivalent performance may be realized

through implementing this approach.[16] Findings indicated that at a pitch of 400 nm cells were aligned and elongated with the ridges, while at a pitch of 4000 nm effects of topography were lost. Similarly, when cells were exposed to flow, those on the 400 nm pitch surfaces adhered more tightly than those on the 4000 nm pitch surfaces. Cells clearly respond to the topography on which they are grown and may be more likely to grow a confluent, fully functional, physiologically similar layer of cells on a surface with which they are familiar.

Recent studies have suggested that that absence of a viable layer of endothelial cells on the basement membrane of bioprosthetic heart valves may be one cause of calcification and subsequent valve failure.[29,30] Hence, incorporation of the natural topography on which aortic heart valve cells grow *in vivo* may prove critical in scaffold design for TEHV. Characterization of basement membrane topography has revealed that this layer is a rich 3-D lattice of nanoscale-sized fibers, pores, and elevations, and through this characterization, important design parameters have been elucidated, thereby providing a rational starting point for design of scaffolds for tissue engineering the aortic valve.

ACKNOWLEDGMENTS

The authors wish to thank the following researchers: Dr. George Abrams, University of Wisconsin-Madison, for her insightful knowledge and advice in planning this study and Kermit Groothius, Dr. Ralph Albrecht, Phil Oschel, Randal Massey, Ben August, and Dr. Nicholas Abbott, University of Wicsonsin-Madison, and Dr. Eadaoin Timmins and Dr. Michael Ball, NCBES, NUI, Galway, for their expertise and assistance in the study. Research carried out by JA Last was supported in part by the Division of Materials Science and Engineering in the Department of Energy Office of Basic Energy Sciences. Sandia is a multiprogram laboratory operated by Sandia Corporation, a Lockheed Martin Company, for the United States Department of Energy under Contract DE-AC04-94AL85000 and is acknowledged for funding J.A. Last. National Institute of Health Grants NEI: EY12253-07 and NIDDK: DK064640-01 partially supported the research. Finally, the Irish Council for Science, Engineering and Technology, funded by the National Development Plan, was the primary sponsor of the research.

REFERENCES

1. Schoen FJ. Approach to the analysis of cardiac valve pros-theses as surgical pathology or autopsy specimens. Cardiovasc. Pathol. 1995; 4:241. [PubMed: 25851087]
2. Flanagan TC, Pandit A. Living artificial heart valve alternatives: a review. Eur. Cell Mater. 2003; 645(28) discussion.
3. Aumailley M, Timpl R. Attachment of cells to basement membrane collagen type IV. J. Cell Biol. 1986; 103:1569. [PubMed: 3771647]
4. Kalluri R. Basement membranes: structure, assembly and role in tumour angiogenesis. Nat. Rev. Cancer. 2003; 3:422. [PubMed: 12778132]
5. Martin GR, Timpl R, Kuhn K. Basement membrane proteins: molecular structure and function. Adv. Protein Chem. 1988; 39:1. [PubMed: 3149870]
6. Abrams GA, Bentley E, Nealey PF, Murphy CJ. Electron microscopy of the canine corneal basement membranes. Cells Tissues Organs. 2002; 170:251. [PubMed: 11919413]
7. Abrams GA, Goodman SL, Nealey PF, Franco M, Murphy CJ. Nanoscale topography of the basement membrane underlying the corneal epithelium of the rhesus macaque. Cell Tissue Res. 2000; 299:39. [PubMed: 10654068]
8. Abrams GA, Murphy CJ, Wang ZY, Nealey PF, Bjorling DE. Ultrastructural basement membrane topography of the bladder epithelium. Urol. Res. 2003; 31:341. [PubMed: 14574540]
9. Abrams GA, Schaus SS, Goodman SL, Nealey PF, Murphy CJ. Nanoscale topography of the corneal epithelial basement membrane and Descemet's membrane of the human. Cornea. 2000; 19:57. [PubMed: 10632010]

10. Den Braber ET, De Ruijter JE, Smits HT, Ginsel LA, von Recum AF, Jansen JA. Effect of parallel surface microgrooves and surface energy on cell growth. J. Biomed. Mater. Res. 1995; 29:511. [PubMed: 7622536]
11. Den Braber ET, De Ruijter JE, Smits HT, Ginsel LA, von Recum AF, Jansen JA. Quantitative analysis of cell proliferation and orientation on substrata with uniform parallel surface microgrooves. Biomaterials. 1996; 17:1093. [PubMed: 8718969]
12. Dalby MJ, Childs S, Riehle MO, Johnstone HJ, Affrossman S, Curtis AS. Fibroblast reaction to island topography: changes in cytoskeleton and morphology with time. Biomaterials. 2003; 24:927. [PubMed: 12504513]
13. Evans MD, Dalton BA, Steele JG. Persistent adhesion of epithelial tissue is sensitive to polymer topography. J. Biomed. Mater. Res. 1999; 46:485. [PubMed: 10398009]
14. Meyle J, Gultig K, Nisch W. Variation in contact guidance by human cells on a microstructured surface. J. Biomed. Mater. Res. 1995; 29:81. [PubMed: 7713962]
15. Barbucci R, Lamponi S, Magnani A, Pasqui D. Micropatterned surfaces for the control of endothelial cell behaviour. Biomol. Eng. 2002; 19:161. [PubMed: 12202177]
16. Karuri NW, Liliensiek S, Teixeira AI, Abrams G, Campbell S, Nealey PF, Murphy CJ. Biological length scale topography enhances cell-substratum adhesion of human corneal epithelial cells. J. Cell Sci. 2004; 117:3153. [PubMed: 15226393]
17. Teixeira AI, Abrams GA, Bertics PJ, Murphy CJ, Nealey PF. Epithelial contact guidance on well-defined micro- and nanostructured substrates. J. Cell Sci. 2003; 116:1881. [PubMed: 12692189]
18. Miller DC, Thapa A, Haberstroh KM, Webster TJ. Endothelial and vascular smooth muscle cell function on poly(lactic-co-glycolic acid) with nano-structured surface features. Biomaterials. 2004; 25:53. [PubMed: 14580908]
19. Goodman SL, Sims PA, Albrecht RM. Three-dimensional extracellular matrix textured biomaterials. Bio-materials. 1996; 17:2087.
20. Murphy, CJ.; Nealey, PF.; Campbell, SF. Substratum topography modulates proliferation of corneal epithelial cells.. The Association for Research in Vision and Ophthalmology 2004 Annual Meeting; Ft. Lauderdale, Florida. 2004;
21. Dalby MJ, Riehle MO, Johnstone H, Affrossman S, Curtis AS. In vitro reaction of endothelial cells to polymer demixed nanotopography. Biomaterials. 2002; 23:2945. [PubMed: 12069336]
22. Chung TW, Liu DZ, Wang SY, Wang SS. Enhancement of the growth of human endothelial cells by surface roughness at nanometer scale. Biomaterials. 2003; 24:4655. [PubMed: 12951008]
23. Spurr SJ, Gibson IK. Isolation of corneal epithelium with Dispase II or EDTA. Invest. Opthalmol. Vis. Sci. 1985; 26:818.
24. Worth Ham, A. Histology. J.B. Lippincott; Philadelphia: 1953. p. 424-426.
25. Bjorling DE, Saban R, Tengowski MW, Gruel SM, Rao VK. Removal of venous endothelium with air. J. Pharmacol. Toxicol. Meth. 1992; 28:149.
26. Jearanaikoon S, Abraham-Peskir JV. An X-ray microscopy perspective on the effect of glutaraldehyde fixation on cells. J. Microsc. 2005; 218:185. [PubMed: 15857380]
27. Deck JD. Endothelial cell orientation on aortic valve leaflets. Cardiovasc. Res. 1986; 20:760. [PubMed: 3791342]
28. Flemming RG, Murphy CJ, Abrams GA, Goodman SL, Nealey PF. Effects of synthetic micro- and nano-structured surfaces on cell behavior. Biomaterials. 1999; 20:573. [PubMed: 10213360]
29. Jansson K, Bengtsson L, Swedenborg J, Haegerstrand A. In vitro endothelialization of bioprosthetic heart valves provides a cell monolayer with proliferative capacities and resistance to pulsatile flow. J. Thorac. Cardiovasc. Surg. 2001; 121:108. [PubMed: 11135167]
30. Eybl E, Griesmacher A, Grimm M, Wolner E. Toxic effects of aldehydes released from fixed pericardium on bovine aortic endothelial cells. J. Biomed. Mater. Res. 1989; 23:1355. [PubMed: 2558116]
1. Fahrenholtz, Monica M.; Wen, Suzanne; Jane Grande-Allen, K. Development of a heart valve model surface for optimization of surface modifications. Acta Biomaterialia. 2015; 26:64–71. [CrossRef]. [PubMed: 26296937]

2. Tu, Chengyi; Das, Subhamoy; Baker, Aaron B.; Zoldan, Janeta; Suggs, Laura J. Nanoscale Strategies: Treatment for Peripheral Vascular Disease and Critical Limb Ischemia. ACS Nano. 2015; 9:3436–3452. [CrossRef]. [PubMed: 25844518]

3. Jeon, Hyeona; Tsui, Jonathan H.; Im Jang, Sue; Lee, Justin H.; Park, Soojin; Mun, Kevin; Chool Boo, Yong; Kim, Deok-Ho. Combined Effects of Substrate Topography and Stiffness on Endothelial Cytokine and Chemokine Secretion. ACS Applied Materials & Interfaces. 2015; 7:4525–4532. [CrossRef]. [PubMed: 25658848]

4. Zhou, Yi; Xiao, Yu; Qiu, Yulei; Yuan, Huipin; van Blitterswijk, Clemens A.; Zhou, Xuedong; Xu, Xiaoming; Bao, Chongyun. Adhesion and proliferation of cells and bacteria on microchip with different surfaces microstructures. Biomedical Engineering / Biomedizinische Technik 0. 2015 [CrossRef].

5. Mestres, Pedro; Lopez Gomez, Laura; Nuñez Lopez, Teresa; del Rosario, Gilberto; Witold Lukas, Slavomir; Hartmann, Uwe. The basement membrane of the isolated rat colonic mucosa. A light, electron and atomic force microscopy study. Annals of Anatomy - Anatomischer Anzeiger. 2014; 196:108–118. [CrossRef]. [PubMed: 24582060]

6. Muhammad R, Lim SH, Goh SH, Law JBK, Saifullah MSM, Ho GW, Yim EKF. Sub-100 nm patterning of TiO 2 film for the regulation of endothelial and smooth muscle cell functions. Biomater. Sci. 2014; 2:1740–1749. [CrossRef].

7. Torrejon, Karen Y.; Pu, Dennis; Bergkvist, Magnus; Danias, John; Sharfstein, Susan T.; Xie, Yubing. Recreating a human trabecular meshwork outflow system on microfabricated porous structures. Biotechnology and Bioengineering. 2013; 110 10.1002/ bit.v110.12, 3205-3218. [CrossRef].

8. Gentile, Francesco; Medda, Rebecca; Cheng, Ling; Battista, Edmondo; Scopelliti, Pasquale E.; Milani, Paolo; Cavalcanti-Adam, Elisabetta A.; Decuzzi, Paolo. Selective modulation of cell response on engineered fractal silicon substrates. Scientific Reports. 2013; 3 [CrossRef].

9. Tocce EJ, Liliensiek SJ, Broderick AH, Jiang Y, Murphy KC, Murphy CJ, Lynn DM, Nealey PF. The influence of biomimetic topographical features and the extracellular matrix peptide RGD on human corneal epithelial contact guidance. Acta Biomaterialia. 2013; 9:5040–5051. [CrossRef]. [PubMed: 23069317]

10. Biggs, Manus; Dalby, Matthew. Shalom WindCellular Response to Nanoscale Features. :461–486. [CrossRef].

11. Das, Manasi. Chandana MohantyNanotechnology for Regenerative Medicine. :297–319. [CrossRef].

12. Wood, Joshua A.; Ly, Irene; Borjesson, Dori L.; Nealey, Paul F.; Russell, Paul; Murphy, Christopher J. The modulation of canine mesenchymal stem cells by nano-topographic cues. Experimental Cell Research. 2012; 318:2438–2445. [CrossRef]. [PubMed: 22771362]

13. Morgan, Joshua T.; Wood, Joshua A.; Shah, Nihar M.; Hughbanks, Marissa L.; Russell, Paul; Barakat, Abdul I.; Murphy, Christopher J. Integration of basal topographic cues and apical shear stress in vascular endothelial cells. Biomaterials. 2012; 33:4126–4135. [CrossRef]. [PubMed: 22417618]

14. Barth, Mareike; Rickelt, Steffen; Noffz, Edeltraut; Winter-Simanowski, Stefanie; Niemann, Heiner; Akhyari, Payam; Lichtenberg, Artur; Wilhelm Franke, Werner. The adhering junctions of valvular interstitial cells: molecular composition in fetal and adult hearts and the comings and goings of plakophilin-2 in situ, in cell culture and upon re-association with scaffolds. Cell and Tissue Research. 2012; 348:295–307. [CrossRef]. [PubMed: 22290634]

15. Li, Yuanyuan; Zhu, Yabin; Yu, Hongwei; Chen, Ling; Liu, Yuxin. Topographic characterization and protein quantification of esophageal basement membrane for scaffold design reference in tissue engineering. Journal of Biomedical Materials Research Part B: Applied Biomaterials. 2012; 100B:265–273. 10.1002/jbm.b.v100b.1 [CrossRef].

16. Hsiao, Ya-Chuan; Lee, Hao-Wei; Chen, You-Tzung; Young, Tai-Horng; Yang, Tsung-Lin. The impact of compositional topography of amniotic membrane scaffold on tissue morphogenesis of salivary gland. Biomaterials. 2011; 32:4424–4432. [CrossRef]. [PubMed: 21439637]

17. Angel, Peggi M.; Nusinow, David; Brown, Chris B.; Violette, Kate; Barnett, Joey V.; Zhang, Bing; Scott Baldwin, H.; Caprioli, Richard M. Networked-based Characterization of Extracellular Matrix Proteins from Adult Mouse Pulmonary and Aortic Valves. Journal of Proteome Research. 2011; 10:812–823. [CrossRef]. [PubMed: 21133377]

18. Tocce EJ, Liliensiek SJ, Wilson MJ, Yanez-Soto B, Nealey PF, MurphyEngineering CJ. the Biophysical Properties of Basement Membranes into Biomaterials: Fabrication and Effects on Cell Behavior. :527–546. [CrossRef].

19. Jonathan Paul Biggs, Manus; Geoff Richards, R.; Dalby, Matthew J. Nanotopographical modification: a regulator of cellular function through focal adhesions. Nanomedicine: Nanotechnology, Biology and Medicine. 2010; 6:619–633. [CrossRef].

20. Khang, Dongwoo; Carpenter, Joseph; Wook Chun, Young; Pareta, Rajesh; Webster, Thomas J. Nanotechnology for regenerative medicine. Biomedical Microdevices. 2010; 12:575–587. [CrossRef]. [PubMed: 19096767]

21. Liliensiek, Sara J.; Wood, Joshua A.; Yong, Jiang; Auerbach, Robert; Nealey, Paul F.; Murphy, Christopher J. Modulation of human vascular endothelial cell behaviors by nanotopographic cues. Biomaterials. 2010; 31:5418–5426. [CrossRef]. [PubMed: 20400175]

22. Pathogenesis of Device-Related Nosocomial Infections. :73–86. [CrossRef].

23. Tocce, Elizabeth J.; Smirnov, Valery K.; Kibalov, Dmitry S.; Liliensiek, Sara J.; Murphy, Christopher J.; Nealey, Paul F. The ability of corneal epithelial cells to recognize high aspect ratio nanostructures. Biomaterials. 2010; 31:4064–4072. [CrossRef]. [PubMed: 20153044]

24. Liliensiek, Sara J.; Nealey, Paul; Murphy, Christopher J. Characterization of Endothelial Basement Membrane Nanotopography in Rhesus Macaque as a Guide for Vessel Tissue Engineering. Tissue Engineering Part A. 2009; 15(9):2643–2651. [Abstract] [Full Text HTML] [Full Text PDF] [Full Text PDF with Links]. [PubMed: 19207042]

25. Uriel, Shiri; Labay, Edwardine; Francis-Sedlak, Megan; Moya, Monica L.; Weichselbaum, Ralph R.; Ervin, Natalia; Cankova, Zdravka; Brey, Eric M. Extraction and Assembly of Tissue-Derived Gels for Cell Culture and Tissue Engineering. Tissue Engineering Part C: Methods. 2009; 15(3): 309–321. [Abstract] [Full Text HTML] [Full Text PDF] [Full Text PDF with Links]. [PubMed: 19115821]

26. Gasiorowski, Joshua Z.; Russell, Paul. Biological properties of trabecular meshwork cells. Experimental Eye Research. 2009; 88:671–675. [CrossRef]. [PubMed: 18789927]

27. Buxton, Denis B. Current status of nanotechnology approaches for cardiovascular disease: a personal perspective. Wiley Interdisciplinary Reviews: Nanomedicine and Nanobiotechnology. 2009; 1:149–155. [CrossRef]. [PubMed: 20049786]

28. Krenning, Guido; Moonen, Jan-Renier A.J.; van Luyn, Marja J.A.; Harmsen, Martin C. Generating New Blood Flow: Integrating Developmental Biology and Tissue Engineering. Trends in Cardiovascular Medicine. 2008; 18:312–323. [CrossRef]. [PubMed: 19345319]

29. Mendonça, Gustavo; Mendonça, Daniela B.S.; Aragão, Francisco J.L.; Cooper, Lyndon F. Advancing dental implant surface technology – From micron- to nanotopography. Biomaterials. 2008; 29:3822–3835. [CrossRef]. [PubMed: 18617258]

30. Fraser, Sarah A.; Ting, Yuk-Hong; Mallon, Kelly S.; Wendt, Amy E.; Murphy, Christopher J.; Nealey, Paul F. Sub-micron and nanoscale feature depth modulates alignment of stromal fibroblasts and corneal epithelial cells in serum-rich and serum-free media. Journal of Biomedical Materials Research Part A. 2008; 86A:725–735. 10.1002/jbm.a.v86a:3 [CrossRef]. [PubMed: 18041718]

31. Norris, Russell A.; Moreno-Rodriguez, Ricardo A.; Sugi, Yukiko; Hoffman, Stanley; Amos, Jenny; Hart, Mary M.; Potts, Jay D.; Goodwin, Richard L.; Markwald, Roger R. Periostin regulates atrioventricular valve maturation. Developmental Biology. 2008; 316:200–213. [CrossRef]. [PubMed: 18313657]

32. Francis, Megan E.; Uriel, Shiri; Brey, Eric M. Endothelial Cell–Matrix Interactions in Neovascularization. Tissue Engineering Part B: Reviews. 2008; 14(1):19–32. [Abstract] [Full Text PDF] [Full Text PDF with Links]. [PubMed: 18454632]

33. Francis, Megan E.; Uriel, Shiri; Brey, Eric M. Endothelial Cell–Matrix Interactions in Neovascularization. Tissue Engineering. 2008; 254:110306233438005. [CrossRef].

34. Dang JM, Leong KW. Myogenic Induction of Aligned Mesenchymal Stem Cell Sheets by Culture on Thermally Responsive Electrospun Nanofibers. Advanced Materials. 2007; 19:2775–2779. 10.1002/adma.v19:19 [CrossRef]. [PubMed: 18584057]

35. Eliason, Marcus T.; Charest, Joseph L.; Simmons, Blake A.; García, Andrés J.; King, William P. Nanoimprint fabrication of polymer cell substrates with combined microscale and nanoscale topography. Journal of Vacuum Science & Technology B: Microelectronics and Nanometer Structures. 2007; 25:L31. [CrossRef].

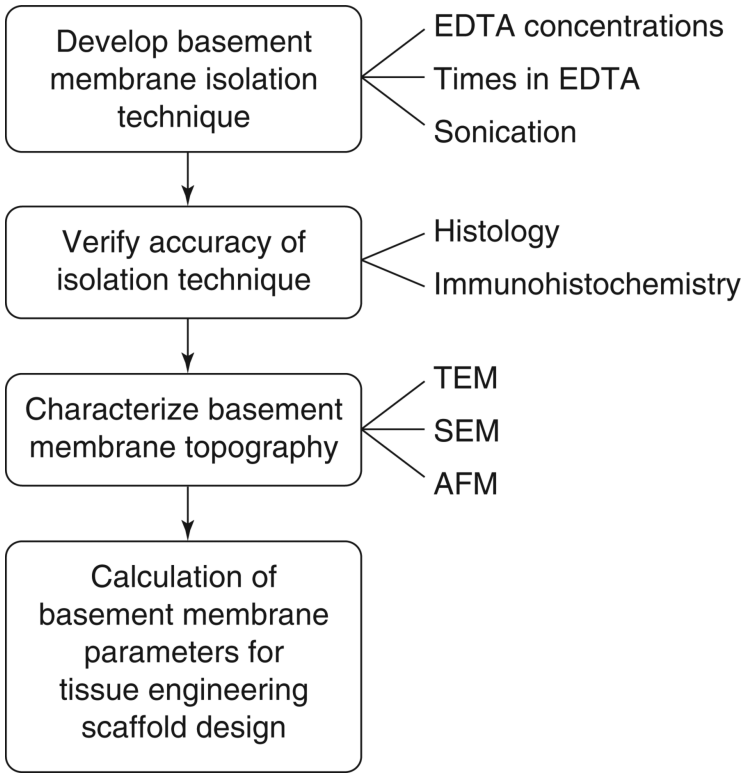

FIG. 1.
Schematic of the steps in characterizing the basement membrane topography of the porcine aortic heart valve.

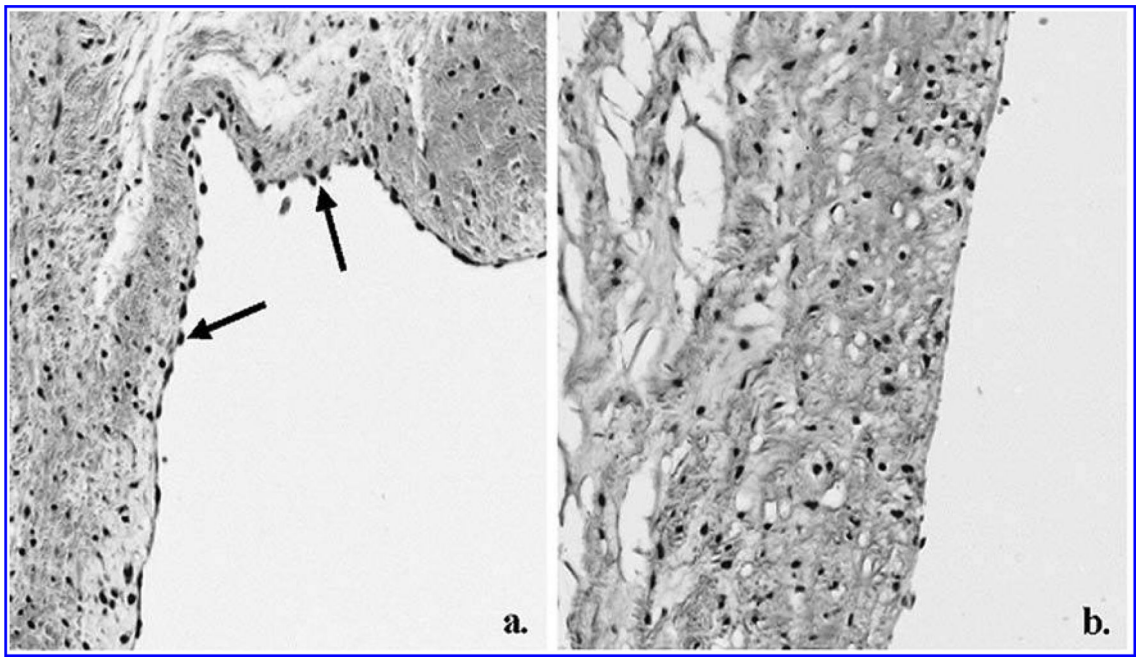

FIG. 2.

Histological sections of control **(a)** and de-endothelialized **(b)** cusps stained with H&E. There is a noticeable absence of endothelial cells on the surface of the de-endothelialized tissue. Cells on the surface of the control are indicated by arrows. (magnification × 200)

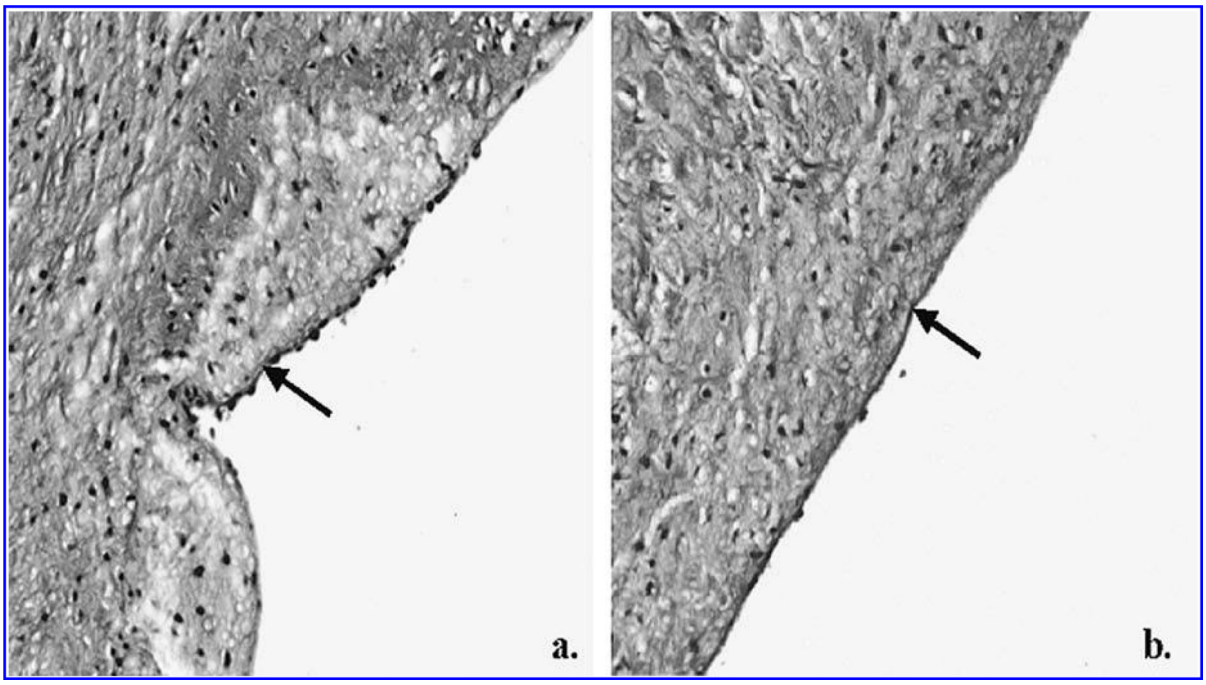

FIG. 3.

Sections of control **(a)** and de-endothelialized **(b)** cusps stained with Alcian blue with periodic acid Schiff. The basement membrane is intact in both cases, as shown by the continuous dark line (indicated by arrows). Note the beaded appearance of the endothelial cells over the basement membrane in **(a)**. (magnification × 200)

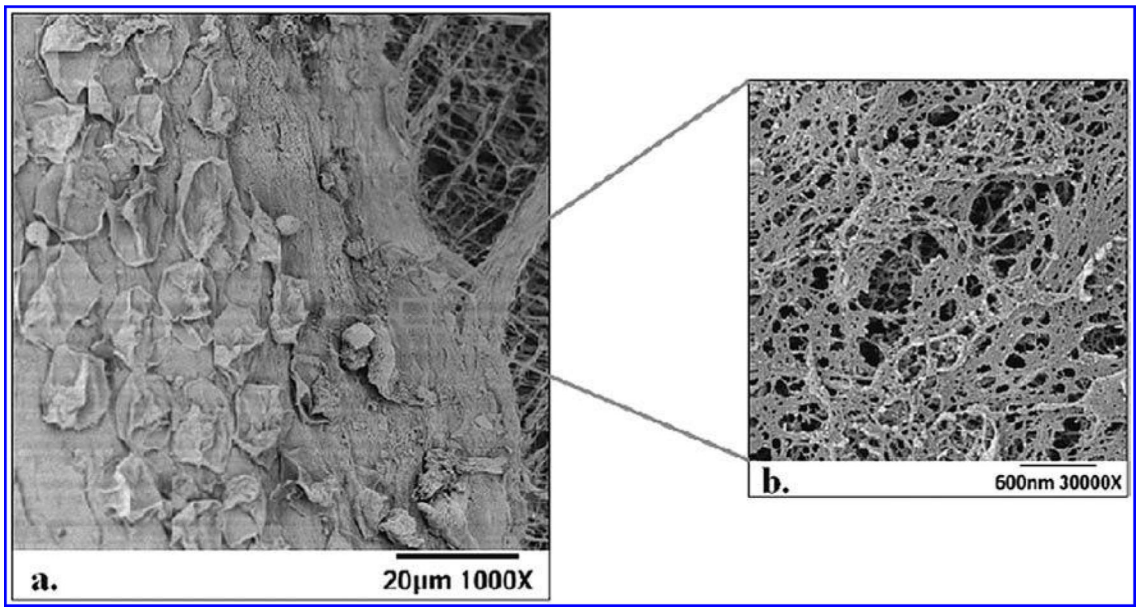

FIG. 4.

(a) SEM micrographs showing the three layers of the aortic valve cusp; some cells are remaining following EDTA treatment, basement membrane, and the underlying extracellular matrix. **(b)** A higher magnification SEM image of the basement membrane, typical of those used for stereo pairs.

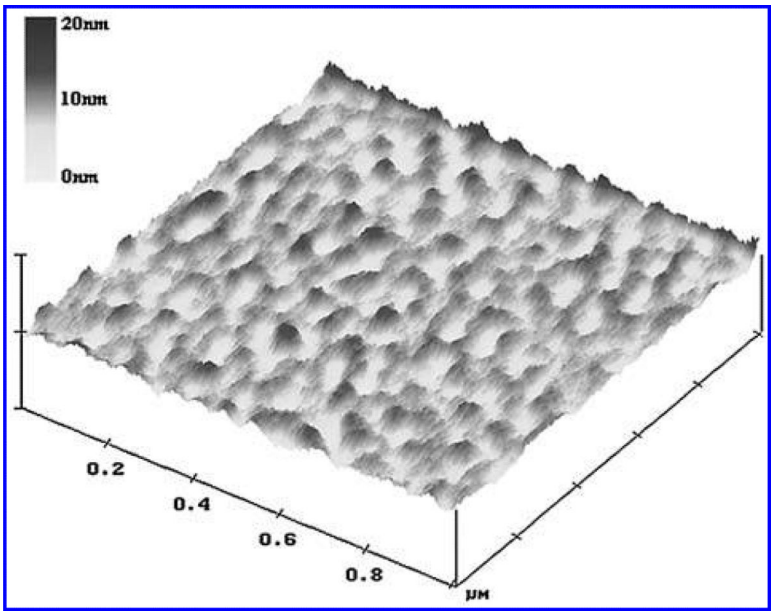

FIG. 5.

A tapping mode atomic force microscopy image of 1 μm^2 area of basement membrane.

Table 1

Comparison Between Basement Membrane Feature Sizes Measured on the Ventricular and Fibrosal Sides of the Heart Valve, Decemet's Membrane in the Human and Canine Cornea,[6,9] and Matrigel[7]

	Matrigel	Descemet's membrane, human	Descemet's membrane, canine	Aortic heart valve ventricular basement membrane, porcine	Aortic heart valve fibrosal basement membrane, porcine
Elevations (SEM)					
Mean ± SD (nm)	162 ± 52	131 ± 41	115 ± 30	26 ± 13	22 ± 11
Range (nm)	76-267	76-229	76-153	7-53	4-71
Pore diameter (SEM)					
Mean ± SD (nm)	105 ± 70	38 ± 15	24 ± 8	32 ± 2	28 ± 4
Range (nm)	26-359	22-87	5-40	12-75	7-98
Fiber diameter (SEM)					
Mean ± SD (nm)	69 ± 35	31 ± 9	15± 7	28 ± 3	30 ± 2
Range (nm)	8-3	18-59	5-44	6-94	9-66
Pore depth (SEM)					
Mean ± SD (nm)				22 ± 13	22 ± 14
Range (nm)				4-57	4-89